Modelling and Experimental Research of Nonholonomic Ball Gear

Bartłomiej Krysiak, Dariusz Pazderski, Krzysztof Kozłowski

Abstract:

The paper considers kinematic and dynamic model of ball gear which can be used in a nonholonomic manipulator. The phase constraints are described and constrained forces and torques are discussed. In order to describe mechanical properties of the gear experimental research were conducted. Based on experimental results maximum driving torque, gear efficiency and resultant slip are estimated.

Keywords: *nonholonomic constraint, nonholonomic manipulator, kinematics and dynamics.*

1. Introduction

Mechanical systems with phase constraints are an important class of objects in robotics. Among of them, one can distinguish systems with kinematic (i.e. first order) constraints which have their roots in pure rolling between bodies in contact or angular momentum preservation principle. If the constraints are not integrable, i.e. they do not reduce size of configuration space, one can call them nonholonomic constraints.

Taking into account robotic applications the most important class of nonholonomic systems constitute majority of wheeled vehicles. Their kinematic structure gives possibility to assume that the motion is not affected by slip phenomenon. Less well known group of nonholonomic robots are nonholonomic manipulators. Their main advantage, at least from a theoretical point of view, is the ability to obtain a lightweight mechanical structure as a result of decreased number of independent actuators with respect to the dimension of manipulator configuration. One of the most familiar proposition of nonholonomic manipulator was given by Sørdalen and others [5]. It is based on ball gears which takes advantage of phase constraints in order to ensure transmission of the torques between joints. The manipulator has been designed and realized in practice in two kinematic versions [1]. In a robotics literature some propositions of continuous and discontinuous control algorithms have been proposed [1–4] to solve regulation and trajectory following tasks. However, not much works have been devoted to analysis of the fundamental part of the manipulator, namely nonholonomic gear.

This paper can be treated as an attempt to fill this gap. It presents detail description of the nonholonomic ball gear taking into account the structure built in the Chair of Control and Systems Engineering, Poznan University of Technology. The idea of mechanism is inspired by proposition presented in [5]. The paper is focused on theoretical description of the gear model including kinematics and dynamics as well and some practical features of the gear. In order to verify fundamental properties of the gear experimental research have been conducted. The results of this research are given in the paper covering maximum value of transmitted torque and overall efficiency of the mechanism.

2. General description of the ball gear

In Figs. 1 and 2 considered mechanism of the nonholonomic gear is presented. It consists of: *ball*, three *active rollers* (input W0 and output W1, W2) which are responsible for torque transmission, and two *passive rollers* W3 and W4, which give support for the ball and exert proper pressure on it needed for torque transmission.

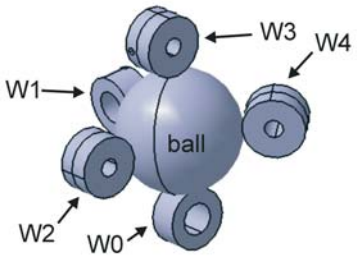

Fig. 1. Visualization of 3D model of the gear structure

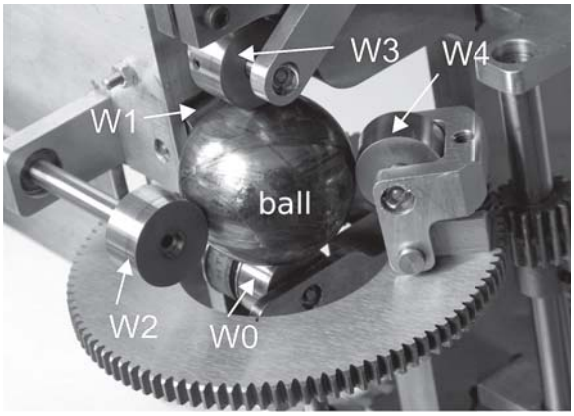

Fig. 2. Picture of the built gear mechanism

The area of contact between input and output rollers and the ball are the source of main phase constraints observed for the gear. Rollers W0 and W3 are placed on the poles of the ball. It is assumed that point contact without slipping exists between each roller and the ball. Direction of the ball rotation is determined by direction of input roller W0 motion. The ball is driven by roller W0 which transmits torque to output rollers W1 and W2. Axes of rollers W1 and W2 lies on a plane of the ball equator. The contacts between the rollers W1 and W2 and the ball creates two constraints

planes. The intersection of those planes determines the rotation axis of the ball. As a result degrees of freedom of the ball becomes reduced to one. Consequently, the ball cannot rotate around axis through its north and south pole. Taking into account that system of associated output rollers can change its orientation with respect to that axis, one can consider angular velocity of the output rollers as a function of an angle between input and output rollers.

3. Analytical model of the gear

In this paper it is assumed that $\boldsymbol{R} \in \mathrm{SO}(3)$ describes any rotation matrix, while

$$\boldsymbol{R}_z(\gamma) \triangleq \begin{bmatrix} \cos\gamma & -\sin\gamma & 0 \\ \sin\gamma & \cos\gamma & 0 \\ 0 & 0 & 1 \end{bmatrix} \in \mathrm{SO}(3) \tag{1}$$

is a matrix denoting rotation around z axis by an angle γ. In order to describe a vector product of two vectors $\boldsymbol{\alpha} = [\alpha_1\ \alpha_2\ \alpha_3]^T \in \mathbb{R}^3$ and $\boldsymbol{\beta} \in \mathbb{R}^3$ the following notation is used:

$$\boldsymbol{\alpha} \times \boldsymbol{\beta} = \boldsymbol{S}(\boldsymbol{\alpha})\boldsymbol{\beta}, \tag{2}$$

where

$$\boldsymbol{S}(\boldsymbol{\alpha}) \triangleq \begin{bmatrix} 0 & -\alpha_3 & \alpha_2 \\ \alpha_3 & 0 & -\alpha_1 \\ -\alpha_2 & \alpha_1 & 0 \end{bmatrix} \in \mathfrak{so}(3) \tag{3}$$

is a skew-symmetric matrix. Unit vectors codirectional with axes of any 3D frame are referred as: $\boldsymbol{e}_1 \triangleq [1\ 0\ 0]^T$, $\boldsymbol{e}_2 \triangleq [0\ 1\ 0]^T$, $\boldsymbol{e}_3 \triangleq [0\ 0\ 1]^T$.

Taking into account the gear model we consider only these components which are relevant for torque transmission, namely the ball and active rollers. Passive rollers which support the ball in this analysis are not taken into account in order to simplify the description. However, these components can be relatively easy included in the model based on presented modeling framework.

3.1. Kinematic description

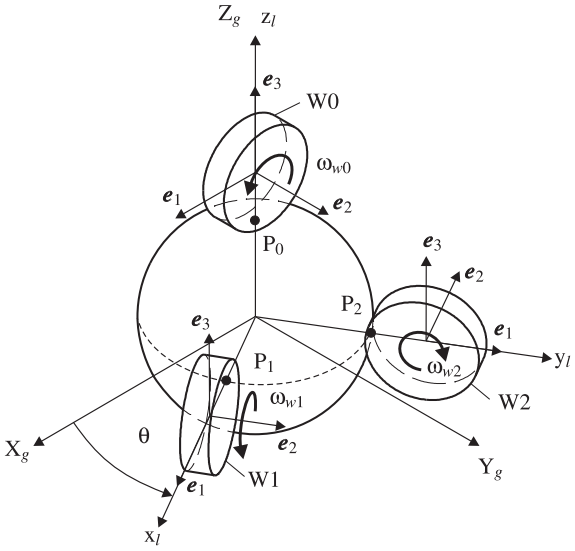

Fig. 3. Geometry of the gear

Let us consider three reference frames with origins placed at center of the ball. The first frame $\mathrm{OX_gY_gZ_g}$ does not change its orientation with respect to inertial one. Axes of the second frame $\mathrm{OX_lY_lZ_l}$ contain points P_0, P_1 and P_2 – this frame rotates in the same way as the system of associated rollers W1 and W2. The third frame is fixed to the ball and it isn't denoted in the figure (3) because of it's clarity reasons. It is assumed that ρ denotes radius of the ball, while r_{w0}, r_{w1} and r_{w2} denote radius of rollers W0, W1 and W2, respectively. Orientation of the ball with respect to the inertial frame is described by rotation matrix $\boldsymbol{R} \in \mathrm{SO}(3)$, while its angular velocity defined in this frame is denoted as $\boldsymbol{\omega} = [\omega_x\ \omega_y\ \omega_z]^T$. Then, time derivative of rotation matrix can be calculated as $\dot{\boldsymbol{R}} = \boldsymbol{S}(\boldsymbol{\omega})\boldsymbol{R}$. Furthermore, we assume that value of angular velocity of i^{th} roller determined in its local frame is described by ω_{wi}.

At the contact point P_0 linear velocity on the ball surface determined in the inertial frame can be written as follows:

$$\dot{\boldsymbol{p}}_0 = \boldsymbol{S}(\boldsymbol{\omega})\boldsymbol{e}_3\rho = [\omega_y\rho\ -\omega_x\rho\ 0]^T, \tag{4}$$

while linear velocity on the roller W_0 surface at the same points equals:

$$\dot{\boldsymbol{p}}_0 = -\boldsymbol{S}(\boldsymbol{e}_2)\boldsymbol{e}_3\omega_{w0}r_{w0} = -\boldsymbol{e}_1\omega_{w0}r_{w0}. \tag{5}$$

Making similar analysis with respect to rollers W1, W2 and the ball at points P_1 and P_2 one obtains:

$$\dot{\boldsymbol{p}}_1 = \dot{\theta}\boldsymbol{S}(\boldsymbol{e}_3)\boldsymbol{R}_z(\theta)\boldsymbol{e}_1\rho - \boldsymbol{R}_z(\theta)\boldsymbol{S}(\boldsymbol{e}_2)\boldsymbol{e}_1\omega_{w1}r_{w1} = \begin{bmatrix} -\dot{\theta}\rho\sin\theta \\ \dot{\theta}\rho\cos\theta \\ \omega_{w1}r_{w1} \end{bmatrix}, \tag{6}$$

$$\dot{\boldsymbol{p}}_1 = \boldsymbol{S}(\boldsymbol{\omega})\boldsymbol{R}_z(\theta)\boldsymbol{e}_1\rho = \begin{bmatrix} -\omega_z\rho\sin\theta \\ \omega_z\rho\cos\theta \\ \omega_x\rho\sin\theta - \omega_y\rho\cos\theta \end{bmatrix}, \tag{7}$$

$$\dot{\boldsymbol{p}}_2 = \dot{\theta}\boldsymbol{S}(\boldsymbol{e}_3)\boldsymbol{R}_z\left(\theta+\tfrac{\pi}{2}\right)\boldsymbol{e}_1\rho - \boldsymbol{R}_z\left(\theta+\tfrac{\pi}{2}\right)\boldsymbol{S}(\boldsymbol{e}_2)\boldsymbol{e}_1\omega_{w2}r_{w2} = \begin{bmatrix} -\dot{\theta}\rho\cos\theta \\ -\dot{\theta}\rho\sin\theta \\ \omega_{w2}r_{w2} \end{bmatrix} \tag{8}$$

and

$$\dot{\boldsymbol{p}}_2 = \boldsymbol{S}(\boldsymbol{\omega})\boldsymbol{R}_z\left(\theta+\tfrac{\pi}{2}\right)\boldsymbol{e}_1\rho = \begin{bmatrix} -\omega_z\rho\cos\theta \\ -\omega_z\rho\sin\theta \\ \omega_x\rho\cos\theta + \omega_y\rho\sin\theta \end{bmatrix}. \tag{9}$$

Next, assuming pure rolling of the roller on the ball and making use of (4)-(9) we get the following equations describing the first order phase constraints:

$$\omega_{w0}r_{w0} + \omega_y\rho = 0, \tag{10}$$

$$-\rho(\omega_x\sin\theta - \omega_y\cos\theta) + \omega_{w1}r_{w1} = 0, \tag{11}$$

$$-\rho(\omega_x\cos\theta + \omega_y\sin\theta) + \omega_{w2}r_{w2} = 0, \tag{12}$$

$$\omega_x = 0, \tag{13}$$

$$\omega_z - \dot{\theta} = 0. \tag{14}$$

Next, defining velocity vector $\boldsymbol{\xi} = [\xi_1\ \xi_2\ \ldots\ \xi_7]^T \triangleq \left[\omega_x\ \omega_y\ \omega_z\ \dot{\theta}\ \omega_{w0}\ \omega_{w1}\ \omega_{w2}\right]^T$ allows one to present the

above constraints in the following Pfaffian form:

$$\boldsymbol{A}(\theta)\,\boldsymbol{\xi} = \boldsymbol{0}, \tag{15}$$

where $\boldsymbol{A}(\theta) \in \mathbb{R}^{5\times 7}$ is the constraint matrix defined as:

$$\boldsymbol{A}(\theta) \triangleq \begin{bmatrix} 0 & \rho & 0 & 0 & r_{w0} & 0 & 0 \\ -\rho \mathrm{s}\theta & \rho \mathrm{c}\theta & 0 & 0 & 0 & r_{w1} & 0 \\ -\rho \mathrm{c}\theta & -\rho \mathrm{s}\theta & 0 & 0 & 0 & 0 & r_{w2} \\ 1 & 0 & 0 & 0 & 0 & 0 & 0 \\ 0 & 0 & 1 & -1 & 0 & 0 & 0 \end{bmatrix} \tag{16}$$

with $\mathrm{s}\theta$ and $\mathrm{c}\theta$ denoting $\sin\theta$ and $\cos\theta$, respectively. Taking into account dimension of vector $\boldsymbol{\xi}$ together with number of independent phase constraints we conclude that considered mechanical system has only two degrees of freedom. Consequently, it implies that one can find two independent vector fields $\boldsymbol{g}_1$ and $\boldsymbol{g}_2$, such that rows of matrix $\boldsymbol{A}$ can be seen as their annihilators. For example these vector fields can be written as follows:

$$\begin{aligned} &\boldsymbol{g}_1 \triangleq [0\,0\;-1\,1\,0\,0\,0]^T, \\ &\boldsymbol{g}_2(\theta) \triangleq \left[0\;-\tfrac{r_{w0}}{\rho}\;0\,0\,1\;\tfrac{r_{w0}}{r_{w1}}\cos\theta\;-\tfrac{r_{w0}}{r_{w2}}\sin\theta\right]^T. \end{aligned} \tag{17}$$

Next, using (17) we can define the following affine system which describes kinematics of the nonholonomic gear:

$$\boldsymbol{\xi} = \boldsymbol{G}(\theta)\,\boldsymbol{u}, \tag{18}$$

where $\boldsymbol{G}(\theta) \triangleq [\boldsymbol{g}_1\ \boldsymbol{g}_2(\theta)]^T \in \mathbb{R}^{7\times 2}$ and $\boldsymbol{u} \triangleq [u_1\ u_2]^T \in \mathbb{R}^2$ is kinematic input vector in the form of quasi-velocities (or alternatively: auxiliary-velocities).

3.2. Dynamic description

Dynamic model of the ball gear will be derived based on Lagrange formalism assuming that potential energy of the system does not change. Then, one can consider the following Lagrangian $\mathcal{L} \triangleq \frac{1}{2}\boldsymbol{\xi}^T\boldsymbol{J}\boldsymbol{\xi}$, where

$$\boldsymbol{J} \triangleq \mathrm{diag}\left\{\tfrac{2}{5}m\rho^2, \tfrac{2}{5}m\rho^2, \tfrac{2}{5}m\rho^2,\ J_l,\ J_{w0},\ J_{w1},\ J_{w2}\right\} \in \mathbb{R}^{7\times 7} \tag{19}$$

is a positive definite symmetric mass matrix, with m denoting mass of the ball, J_l being inertia of the output rollers system determined around $\mathrm{Z_g}$ axis, while J_{wi} determines inertia of i^{th} rollers around its axis of rotation.

The control input is considered as torques applied to roller W0 and the system of rollers W1 and W2, and it is described by $\boldsymbol{\tau} \triangleq [\tau_1\ \tau_2]^T \in \mathbb{R}^2$. Additionally external torques (disturbances) denoted by $\boldsymbol{\tau}_z \triangleq [\tau_{z1}\ \tau_{z2}\ \tau_{z3}\ \tau_{z4}]^T \in \mathbb{R}^4$ are considered. These torques can be seen mainly as a result of the torque transmission to the components of mechanism external to the gear (for example links of a manipulator, interaction with an environment, etc.) as well as some internal friction effects (including rolling friction on the ball surface and friction which appears in bearings of the rollers).

Calculating inertia generalized forces as $\frac{d}{dt}\left(\frac{\partial \mathcal{L}}{\partial \dot{\boldsymbol{\xi}}}\right)^T = \boldsymbol{J}\dot{\boldsymbol{\xi}}$, considering input $\boldsymbol{\tau}$, disturbances $\boldsymbol{\tau}_z$ and phase constraints interactions, and referring to d'Alemberd principle

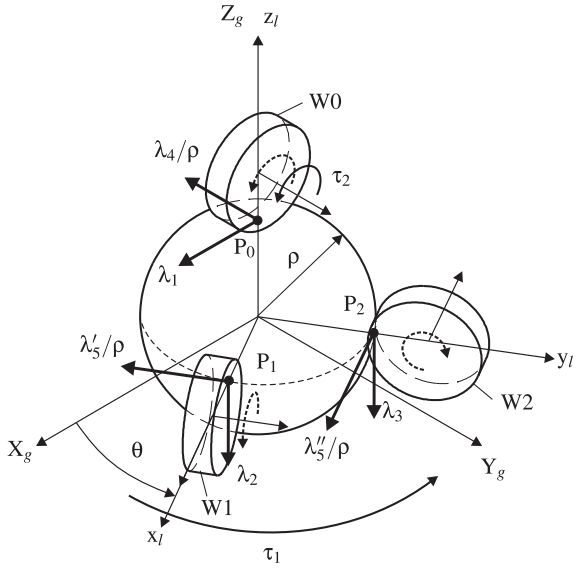

Fig. 4. Forces and torques in the gear

and Lagrange equation one can derive the following dynamics of the gear:

$$\boldsymbol{J}\dot{\boldsymbol{\xi}} = \boldsymbol{B}\boldsymbol{\tau} + \boldsymbol{B}_z\boldsymbol{\tau}_z + \boldsymbol{Q}_w, \tag{20}$$

where

$$\begin{aligned} \boldsymbol{B} &\triangleq \begin{bmatrix} 0 & 0 & 0 & 1 & 0 & 0 & 0 \\ 0 & 0 & 0 & 0 & 1 & 0 & 0 \end{bmatrix}^T, \\ \boldsymbol{B}_z &\triangleq \begin{bmatrix} 0 & 0 & 0 & 1 & 0 & 0 & 0 \\ 0 & 0 & 0 & 0 & 1 & 0 & 0 \\ 0 & 0 & 0 & 0 & 0 & 1 & 0 \\ 0 & 0 & 0 & 0 & 0 & 0 & 1 \end{bmatrix}^T \end{aligned} \tag{21}$$

are input matrices (related to control input and disturbances, respectively),

$$\boldsymbol{Q}_w = [Q_{w1}\ Q_{w2}\ \ldots\ Q_{w7}]^T = \boldsymbol{A}^T(\theta)\,\boldsymbol{\lambda} \tag{22}$$

denotes generalized forces of the phase constraints, with $\boldsymbol{\lambda} \in \mathbb{R}^5$ determining vector of Langrange multipliers.

Taking advantage of kinematics (18) allows one to present dynamics equation (20) in the following reduced form:

$$\bar{\boldsymbol{M}}\dot{\boldsymbol{u}} + \bar{\boldsymbol{C}}\boldsymbol{u} = \bar{\boldsymbol{B}}\boldsymbol{\tau} + \bar{\boldsymbol{B}}_z\boldsymbol{\tau}_z, \tag{23}$$

where $\bar{\boldsymbol{M}} = \boldsymbol{G}^T\boldsymbol{J}\boldsymbol{G}$, $\bar{\boldsymbol{C}} = \boldsymbol{G}^T\boldsymbol{J}\dot{\boldsymbol{G}}$, $\bar{\boldsymbol{B}} = \boldsymbol{G}^T\boldsymbol{B}$ and $\bar{\boldsymbol{B}}_z = \boldsymbol{G}^T\boldsymbol{B}_z$. Vector of Lagrange multipliers can be calculated from the following relationship:

$$\boldsymbol{\lambda} = -\left(\boldsymbol{A}\boldsymbol{J}^{-1}\boldsymbol{A}^T\right)^{-1}\left(\dot{\boldsymbol{A}}\boldsymbol{\xi} + \boldsymbol{A}\boldsymbol{J}^{-1}\left(\boldsymbol{B}\boldsymbol{\tau} + \boldsymbol{B}_z\boldsymbol{\tau}_z\right)\right). \tag{24}$$

Making analysis of the term (22) one can find physical interpretation of individual components of vector $\boldsymbol{\lambda}$. Then, fulfillment of the constraints imply that:

$$Q_{w5} = r_{w1}\lambda_1,\ Q_{w6} = r_{w2}\lambda_2,\ Q_{w7} = r_{w3}\lambda_3, \tag{25}$$

$$Q_{w3} = -Q_{w4} = \lambda_5 \tag{26}$$

and

$$Q_{w1} = -\rho\left(\sin\theta\cdot\lambda_2 + \cos\theta\cdot\lambda_3\right) + \lambda_4. \tag{27}$$

Next, considering Fig. 4 and taking into account (25), (26) allows one to make the following statements:

– λ_1, λ_2 and λ_3 multipliers determine lateral components of interaction forces between rollers W0, W1, W2 and the ball – cf. equation (25).
– λ_4 multiplier determines torque constraint coming from lack of the ball rotation around X_g axis – cf. equation (27); it is generated by lateral component of force interaction between the roller W0 and the ball,
– λ_5 multiplier denotes torque constraint, which results from lack of relative rotation of the ball with respect to the system of output rollers W1 and W2 around Z_g axis – cf. equation (26); it is caused by lateral components of resultant forces between rollers W1, W2 and the ball (value of these components can be denoted by λ_5'/ρ and λ_5''/ρ, with $\lambda_5' + \lambda_5'' = \lambda_5$).

It is worth to note that the constraints forces and torques coming form interactions between components of the gear and their maximum magnitudes are physically limited by permissible friction forces. Considering Fig. 4 we can find the following inequalities

$$\sqrt{\lambda_1^2 + \frac{\lambda_4^2}{\rho^2}} \leq F_{w0\,\max}, \sqrt{\lambda_2^2 + \frac{\left(\lambda_5'\right)^2}{\rho^2}} \leq F_{w1\,\max}, \sqrt{\lambda_3^2 + \frac{\left(\lambda_5''\right)^2}{\rho^2}} \leq F_{w2\,\max}, \tag{28}$$

where $F_{wi\,\max} = \mu_i N_i$ denotes maximum force friction which results from contact force N_i between i^{th} roller and the ball and μ_i is the Coulumb friction coefficient, with $i = 0, 1, 2$.

4. Experimental research on nonholonomic gear

Mathematical model of the nonholonomic gear presented in Section 3 is relatively complicated. The main difficulty is a determination of friction coefficients, due to many mechanical elements. In practice it is hard to define these parameters because they are related with many variables such as pressure force, kind of material and wear and tear of material.

Taking into account practical aspects in a sense of application of the nonholonomical gear we are interested to know the maximum transmission driving moment and the efficiency of transmission. Concerning the method of transmission drive, occurrence of a skid between the ball and roller becomes also very important issue. Its appearance means that constraints described by equation (15) are violated. These problems were experimentally examined.

4.1. Experiment description

Experimental workstation consists of one joint of a manipulator using the nonholonomic gear and electrical driving and braking system – see Figs. 5 and 6. The gear is driven by motor[1] MN. Planetary gear integrated with this motor transforms drive torque $\tau_N = \tau_2$ to W0 roller with use of toothed belt. The output roller W2, which receives torque, is coupled with identical motor MH which is a braking motor. This motor works in generator mode and provides resistance torque $\tau_{z4} = -\tau_H$.

In order to determine characteristic of resistances which occurs in motor, planetary gears, driving toothed belt and

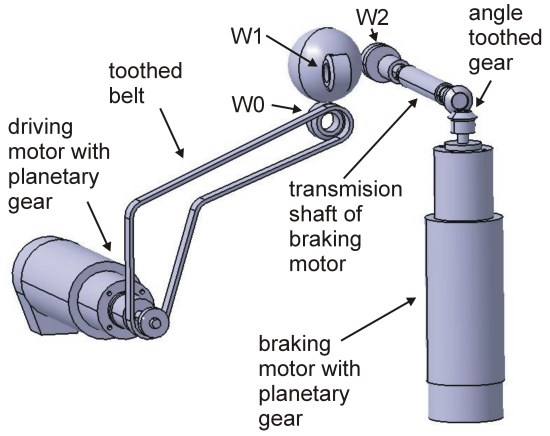

Fig. 5. Model of experimental setup – the gear coupled with drive and brake

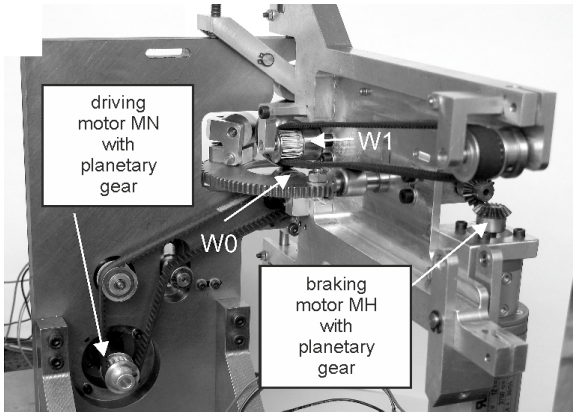

Fig. 6. The real experimental setup

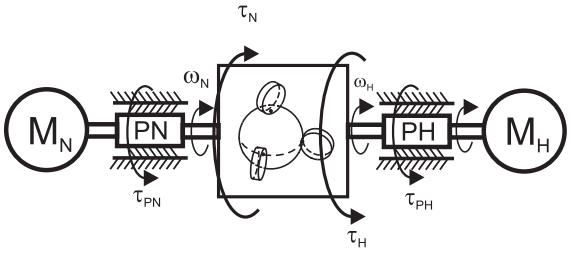

Fig. 7. Block schema of driving and braking system

in transmission shaft (indicated in Fig. 7) tests of neutral (i.e. no loaded on the input or output side) gear were carried out separately for driving system and for braking system. The driving system consists of electrical motor, planetary gear and transmission system with toothed belt. The braking system consists of second electrical motor, planetary gear, transmission system with transmission shaft and angle toothed gear. From linear regression the resistance torque characteristics were carried out with use of current measurement and angle velocity measurement (τ_{PN} for driving system and τ_{PH} for braking system).

$$\tau_{PN} = (0.0037\omega_N + 0.42)\, k_i n, \tau_{PH} = = (0.0018\omega_H + 0.18)\, k_i n, \tag{29}$$

where $k_i = 0.09$ Nm/A is the engine electromechanical constant assumed on the basis of catalog data [2], $n = 4.5$

is the ratio of reducing gear integrated with engines and $\omega_N = \omega_{w0}, \omega_H = \omega_{w2}$ are angular velocities calculated in $[\mathrm{rad/s}]$. Angular velocities of the rollers were measured with use of the pulse angular position sensor integrated with engines. Estimation of torques τ_N and τ_H was based on assumed torque resistance characteristics and motor currents.

In experiments roller WO exerted around 80N pressure force on the ball and roller W2 exerted pressure force around 40N. These forces were calculated based on known construction of used holdfast springs. Considering determination uncertainty of Young module and manufacture imprecision of dimensions for used springs it is worth to mark that forces are calculated with high inaccuracy. The radius of rollers WO and W2 are identical and equal $r_{w0} = r_{w2} = 10$ mm.

For identification of *relative skid* during torque transmission from roller W0 to roller W2 we consider kinematic equations (17) and (18). Then, we obtain

$$\omega^*_{w0} = -\frac{r_{w2}}{r_{w0}\sin\theta}\omega_{w2} \cdot 100\,[\%]\,, \tag{30}$$

where ω^*_{w0} is interpreted as the transformed velocity ω_{w2} on the input side of nonholonomic gear. The relative skid is defined as

$$\sigma = \frac{\omega_{w0} - \omega^*_{w0}}{\omega_{w0}} \cdot 100\,[\%]\,. \tag{31}$$

Substituting equation (30) in (31) we have[3]

$$\sigma = \frac{\omega_{w0} + \frac{r_{w2}}{r_{w0}\sin\theta}\omega_{w2}}{\omega_{w0}} \cdot 100\,[\%]\,. \tag{32}$$

Further taking into account the same radius of r_{w0} and r_{w2} relation (32) can be simplified as follows

$$\sigma = \frac{\omega_{w0} + \sin^{-1}(\theta)\,\omega_{w2}}{\omega_{w0}} \cdot 100\,[\%]\,. \tag{33}$$

It is worth to note that using this method of skid estimation does not allows one to determine if it appears between input roller W0 and the ball, or between the ball and the output roller W2. Instead of this we get only measure of resulting slip, which is the most important from a practical point of view.

The gear efficiency is considered with respect to power and torque transmission and is described using the following two factors:

$$\eta_P \triangleq \frac{P_N}{P_H} \cdot 100\,[\%]\,, \qquad \eta_\tau \triangleq \frac{\tau_N}{\tau_H} \cdot 100\,[\%]\,, \tag{34}$$

where $P_N \triangleq \omega_N \tau_N$ and $P_H \triangleq \omega_H \tau_H$ denote input and output mechanical power, respectively.

4.2. Results of experiments

The experiments conducted for the nonholonomic gear were realized for fixed value of angle θ with constant angular velocity $\omega_{w0} = 23\ \mathrm{rad/s}$ (the velocity was stabilized by an industrial PID motor controller).

The first experiment was performed for joint angle $\theta = -\frac{\pi}{2}$. From Fig. 8 one can observe that braking torque range is limited to $\tau_{Hmax} = 0.13$ Nm. Exceeding this value of torque output roller starts to slide on the ball and the gear does not transmit the torque anymore. In the range of normal operation of the gear, the increase of braking torque load causes the increase of relative skid between the rollers and the ball. For the value τ_{Hmax} the relative skid σ was equal 5%. Figure 9 presents power efficiency η_P and torque efficiency η_τ as a function of τ_H. With the increase of torque τ_H the efficiency η_P and η_τ also increases. Increasing the braking torque by 0.11 Nm causes increasing of the efficiency factor by 13%. Probably it asise from increasing roller tension force applied on the ball caused by greater gear load appearance. Very small bearing backlash and bearings resistance forces may cause partial transformation of a rotation moment into holdfast force, which grows while gear moment load increases. It can be observed that η_P efficiency changs in a similar way as η_τ efficiency, but while load force increased up to τ_{Hmax} there appears diversification between these two quantities. For the value τ_{Hmax} coefficient η_P is 4% smaller then η_τ. It results from the growth of skid for larger values of τ_H.

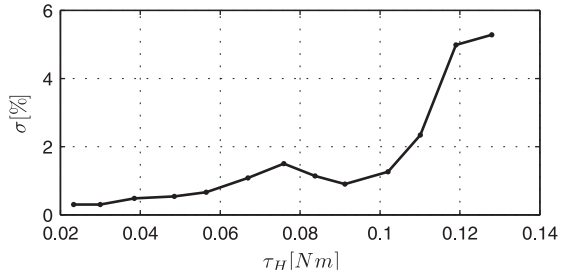

Fig. 8. Gear skid as a function of load force for the angle $\theta = -\frac{\pi}{2}$

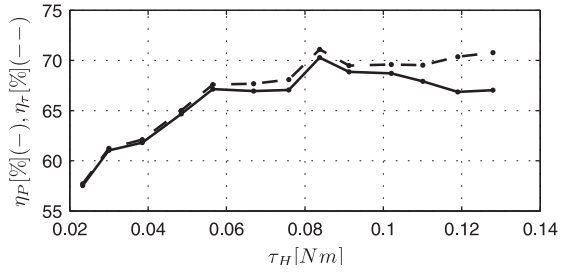

Fig. 9. Gear efficiency as a function of load force for the angle $\theta = -\frac{\pi}{2}$

The second experiment was carried out for a different configuration of the gear, namely $\theta = \frac{\pi}{4}$. In this case torque τ_H is restricted to $\tau_{Hmax} = 0.083$ Nm – cf. Fig. 10. Similarly as in the first experiment with the growth of τ_H relative skid also increases up to maximum value $\sigma = 6.2\%$. From the analysis of efficiency graph (see Fig. 11) also arises empirical statement that for the growth of τ_H the efficiency η_P and efficiency η_τ grows. Torque τ_H rises by 0.08 Nm and causes about 20% efficiency increase. This relation is similar to one observed for the first experiment and we conclude that it is caused by the same reason as in the experiment taken for $\theta = -\frac{\pi}{2}$. Change of efficiency η_P in comparison to efficiency η_τ as a function of moment τ_H shows that η_P has a bigger increase, what also results from growth of relative skid σ as a function of τ_H.

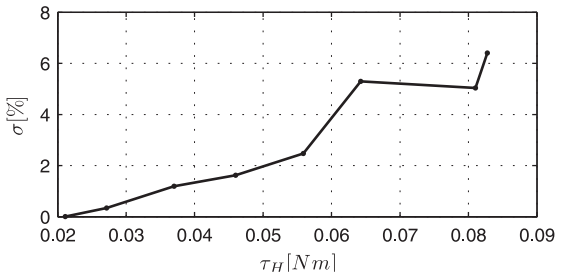

Fig. 10. Gear skid as a function of load force for the angle $\theta = \frac{\pi}{4}$

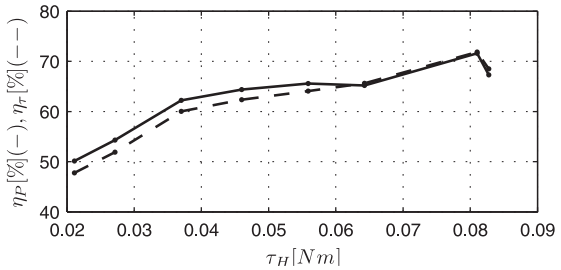

Fig. 11. Gear efficiency as a function of load force for the angle $\theta = \frac{\pi}{4}$

From comparison of experimental results for different values of angle θ we can say that relative skid was more or less 1% bigger for experiment with angle $\theta = \frac{\pi}{4}$. Concerning small difference of relative skid for both experiments it can be stated that changes of angle θ do not influence significantly skid between rollers and the ball. It leads to conclusion that efficiency of the gear is not related to value of angle θ. These results confirm the symmetry of the gear. The same conclusion can be obtained from comparison of efficiency obtained for two different angles. The difference between efficiencies η_P for angle $\theta = -\frac{\pi}{2}$ and for angle $\theta = \frac{\pi}{4}$ is at the level of 0.3%, and difference between efficiencies η_τ for angle $\theta = -\frac{\pi}{2}$ and for angle $\theta = \frac{\pi}{4}$ is at the level of 1.5%.

5. Conclusions

This article presents model analysis and experimental tests of nonholonomic ball gear. Nonholonomic gear mechanism built in the Chair of Control and System Engineering was introduced. Mathematical modeling was considered at a level of kinematics and dynamics pointing out physical interpretation of generalized constraint forces.

Experimental research described here gave possibility to verify properties of the gear in practice as well as to prepare some modifications in the mechanism in order to improve it. The results show some limitations of the examined gear taking into account maximum values of transmitted torque and power. In spite of them one can expect that the properties of the gear should be satisfactory enough to find application of it in a construction of small planar nonholonomic manipulator.

Acknowledgment

This work was supported by the Ministry of Science and Higher Education grant No. N514 299735.

AUTHORS
Bartłomiej Krysiak* – Chair of Control and Systems Engineering, Poznań University of Technology, ul. Piotrowo 3a, 60–965 Poznań, POLAND, e-mail: bartlomiej.krysiak@put.poznan.pl, www: http://control.put.poznan.pl/pl/users/bartlomiejkrysiak
Dariusz Pazderski – Chair of Control and Systems Engineering, Poznań University of Technology, ul. Piotrowo 3a, 60–965 Poznań, POLAND, e-mail: dariusz.pazderski@put.poznan.pl, www: http://etacar.put.poznan.pl/dariusz.pazderski
Krzysztof Kozłowski – Chair of Control and Systems Engineering, Poznań University of Technology, ul. Piotrowo 3a, 60–965 Poznań, POLAND, e-mail: krzysztof.kozlowski@put.poznan.pl, www: http://control.put.poznan.pl
* Corrresponding author

References

[1] W. Chung. *Nonholonomic manipulators*. Springer-Verlag, Berlin Heidenberg, 2004.

[2] A. Mazur and Ł. Nocek. Trajectory tracking for rigid 3-pendulum with nonholonomic gears. In *Proc. of the Fith International Workshop on Robot Motion and Control*, pages 187–192, June 2005.

[3] Y. Nakamura, W. Chung, and O. J. Sørdalen. Design and control of the nonholonomic manipulator. *IEEE Transactions on Robotics and Automation*, 17(1):48–59, February 2001.

[4] D. Pazderski, K. Kozłowski, and K. Krysiak. Nonsmooth stabilizer for three link nonholonomic manipulator using polar-like coordinate representation. In *Lecture Notes in Control and Computer Sciences*, pages 35–44. Springer-Verlag, Berlin Heidenberg, 2009.

[5] O. J. Sørdalen, Y. Nakamura, and W. Chung. Design of a nonholonomic manipulator. In *Proc. of the IEEE Int. Conf. on Robotics and Automation*, pages 8–13, August 1994.

Notes

[1] In tests was used DC motor GR42x20 made by Dunkermotoren.

[2] A value of constant k_i additionally was confirmed by tests with use of dynamometer sensor DFM22-5.0 made by Megatron.

[3] Lack of sign "–" in numerator in expression (31) comes from definition convention of velocity sign for ω_{w2} and ω_{w0}.